Supporting Information

Dimitriu et al. 10.1073/pnas.1406840111

SI Text

Plasmids and Strains. The background strain JC1191 (1) has the genotype *att::rhl-catLVA(Sp^R) ΔsdiA::FRT rrnB3 ΔlacZ4787 hsdR514 Δ (araBAD)567 Δ (rhaBAD)568 rph-1*. The att::rhl-catLVA(Sp^R) segment contains both an Rhl auto-inducer-responsive promoter (P_{rhl*}) driving an unstable version of *cat* [providing chloramphenicol (Cm) resistance], and the *rhlR* gene under the weak constitutive promoter P_{lacI}^q. This cassette is integrated into the chromosome with the spectinomycin resistance Sp^R. Therefore, the growth of JC1191 in Cm is strongly dependent on the Rhl autoinducer C_4-HSL: when present in sufficient concentration in the growth medium, C_4-HSL binds to the RhlR receptor and induces the expression of Cm resistance.

P$^+$ and P$^-$ plasmids are low-copy plasmids with pSC101* replication origin. P$^+$ plasmid carries an artificial operon of *YFP* and *rhlI* (separated by a Shine–Dalgarno translation signal) under control of the strong promoter P_R. RhlI produces the Rhl autoinducer C_4-HSL (1). P$^-$ plasmids carry *GFP* under control of P_R. P$^+$-bearing cells are public good producers, P$^-$-bearing cells are nonproducers.

To provide transfer ability, all cells bear the helper plasmid F_{HR}. F_{HR} is a mutant of pOX38::Tc (2), where *oriT* contains two substitutions (A141T and C144G) that reduce binding and mobilization efficiency by the F relaxase compared with the wild-type F sequence (3). F_{HR} also bears a deletion of the *traS* gene: as TraS protein is responsible for the major part of entry exclusion of F plasmid (4), recipient cells bearing F_{HR} are able to receive T$^+$ plasmids efficiently, and behave as secondary donors. F_{HR} has strongly reduced self-transfer compared with F (1,000-fold reduction) but efficiently mobilizes *oriT*-bearing plasmids. The F_{HR} plasmid thus provides efficient mobilization of T$^+$ plasmids present in the cell, which carry the wild-type *oriT* sequence of F plasmids. Both P$^+$ and P$^-$ plasmids have T$^+$ versions with *oriT*.

Recipients (R) bear pSB3K3-RFP, a medium-copy plasmid with p15A replication origin, carrying *mRFP1* under control of the strong promoter P_{lacI}. Recipients can receive T$^+$ plasmids (T$^+$P$^+$ and T$^+$P$^-$ plasmids) but do not carry them initially: mRFP1 red fluorescence thus identifies recipient cells and secondary plasmid bearers brought by transfer from initial T$^+$-bearing cells to R cells.

P$^+$, P$^-$, and pSB3K3-RFP plasmids are maintained with kanamycin resistance genes.

Genotypes and relevant phenotypes of competitor plasmids and their identification by flow cytometry are summarized in Fig. S1.

Plasmids and Strains Construction. To construct P$^+$ plasmid used in our experiments, the YFP coding sequence (5) was amplified and cloned in pZS*2R-GFP,rhlI (1), replacing GFP. To construct P$^-$ plasmid, pZS*2R-GFP,rhlI was digested with HindIII and XbaI and religated with the linker sequence AGCTTAATTAGCTGAGTCTAG to remove *rhlI*. T$^+$ plasmids were constructed by amplifying *oriT* from the F plasmid (coordinates 66002–66494 from GenBank NC_002483) and inserting it in the common SacI site of P$^+$ and P$^-$ plasmids, in direct orientation. pSB3K3-RFP plasmid was obtained from the Registry of Standard Biological Parts (6).

F_{HR} plasmid was made in two steps. The first one was allelic exchange of pOX38::Tc (2) with a modified F *oriT* including mutations A141T and C144G, following the nomenclature in ref. 3. This mutated *oriT* was first cloned into the SacI site of pDS132 plasmid (7), then integrated in pOX38::Tc by allelic exchange with the wild-type sequence (7). In the second step, F_{HR} plasmid was obtained by deleting *traS* gene using λ/red homologous recombination (8): the sequence between F coordinates 88274 and 88606 was replaced by the *cat* cassette from pKD3, which was then removed with pCP20 (8). F_{HR} plasmid was transferred by conjugation to all strains needed, as it retains low conjugation ability.

Growth Conditions. Cells were grown in Luria-Bertani (BD Difco) medium with 25 μg/mL spectinomycin (Sp, Sigma-Aldrich) and 50 μg/mL kanamycin (Kn, Sigma-Aldrich), and with or without 6.25 μg/mL Cm (Sigma-Aldrich) and 0.75 μM C4-HSL. Experiments were conducted under well-mixed conditions with 5 mL medium in 50-mL tubes (Sarstedt).

For experiments involving public good benefits (all except Fig. 2), 0.75 μM C_4-HSL (CAS# 67605–85-0, Cayman Chemical) was added to the medium from the 30 °C-dilution step, as P$^+$ were found to outcompete P$^-$ at low initial proportions, suggesting a differential benefit of low public good concentrations for producers; 0.75 μM C_4-HSL (mimicking the production of 2.5% P$^+$-bearing cells) restored the apparent cost of P$^+$, maintaining the configuration of the system in a state where cooperation is costly.

Note that markers are not stably maintained after transfer, as both T$^+$ and pSB3K3-P_{lacI}-RFP plasmids bear Kn-resistance markers, and one of the plasmids could be lost without the loss of resistance of the cell. However, this problem is minimized in our experimental setup: both types of plasmids are compatible, as they have different replication origins, and cells are cultured only for a short time period after the transfer actually happens. Despite potential for long-term marker loss, RFP fluorescence still accurately identifies cells on the timescale of our experiments. Indeed, we see no shift in the red fluorescence signal of transconjugants (that stays clearly distinct from the one of donor cells) compared with recipients during our experiments (Fig. 1*B*).

Flow Cytometry Analysis. Cultures were analyzed for strain and plasmid proportions by flow cytometry at t_0 and t_1 for experiments not involving public good benefits (Fig. 2), and at t_1 and t_2 for all other experiments. In the latter case, global proportions at the metapopulation scale were also measured by pooling equal volumes of each population.

For flow cytometry analysis of plasmid and strain proportions, cultures were fixed in 1% formaldehyde (Thermo Scientific) for 10 min, then resuspended in PBS (Life Technologies) and stored at 4 °C. Data acquisition was performed at the Cochin Cytometry and Immunobiology Facility. For each sample, 50,000 cells (increased to 100,000 cells when some competitors were present in proportions <1%) were analyzed using a LSRFortessa cell analyzer (BD Biosciences) with 405-, 488-, and 561-nm excitation lasers. Data analyses were performed using FlowJo (TreeStar). Recipients were identified with RFP, P$^+$ plasmids with YFP, and P$^-$ plasmids with GFP fluorescence (Fig. S1). Cells with double RFP+YFP or RFP+GFP fluorescence were thus recipients that received, respectively, P$^+$ and P$^-$plasmids. After gating on forward and side scattering, three populations were first separated based on 530/30-nm and 670/30-nm filters (Fig. 1*C*, *Left*): P = (P$^+$, P$^-$), R and RP = (RP$^+$, RP$^-$). Then, P$^+$ and P$^-$ cells in two of the populations were distinguished based on 530/30-nm and 525/50-nm filters, separating GFP and YFP (Fig. 1*C*, *Right*).

Whereas transfer can happen from T$^+$-plasmid-bearing cells to any of the cells present, our experimental setup ensured transfer would happen mainly to R cells. T$^+$-plasmid–bearing cells were

placed in very low initial proportions, making transfer to other T^+-bearing cells rare. Double GFP+YFP positive cells, arising either from transfer between T^+-bearing cells or from transfer of both P^+ and P^- plasmids to R cells, represented less than 2% of all cells analyzed and were excluded from the analysis.

Data Analysis. ***Selection of cooperation.*** As both plasmids increase in proportion with transfer, we estimate the relative success of the producer allele as P^+ change in proportion relatively to P^-, $P^+/(P^- + P^+)$ excluding recipients that do not bear P^+ or P^- plasmids. The global ratio at the metapopulation level was measured by pooling equal volumes of populations, effectively taking into account differential growth among populations. The mean ratio was computed as the mean of ratios within populations, to exclude this effect of differential growth.

We did not evaluate absolute changes experimentally, as optical density measurements evaluating absolute changes in cell density were found not to be accurate, potentially because of the aggregation of highly piliated cells, which may vary depending on the growth phases and experimental conditions.

To quantify the difference of within- and among-population ratios in a normalized way across experiments, we computed a coefficient a that represents how biased the global ratio is compared with a nonstandardized mean of populations (the bias arising from differential growth). Let Y_1 and Y_2 be, respectively, ratios in the producer-poor and producer-rich subpopulations, and Y_m the global ratio at the metapopulation level after mixing the two subpopulations. The coefficient a satisfies the equation $Y_m = [(1-a)Y_1 + (1+a)Y_2]/2$, and is thus defined as $a = (2Y_m - Y_1 - Y_2)/(Y_2 - Y_1)$.

Relatedness. In the main text we have already described the measure of genetic assortment, relatedness $\beta_{G,g}$. Here we provide a precise, numerical definition of the relatedness of P^+, $\beta^p_{G,g}$.

Let p_i and n_i be, respectively, the proportion of producers and number of bacteria within subpopulation i, and p_{tot} and n_{tot} be, respectively, the proportion of producers and number of bacteria in the metapopulation. Then, assuming populations are of the same size, which is the case at t_1, the relatedness of producers $\beta^p_{G,g}$ can be calculated as follows from the regression definition of relatedness (9):

$$\beta^p_{G,g} = \left(\sum_i \frac{p_i}{n_i} \frac{p_i}{p_{tot}} - \frac{p_{tot}}{n_{tot}} \right) \Big/ \left(1 - \frac{p_{tot}}{n_{tot}} \right).$$

To compute relatedness for nonmobile loci, we applied the same formula, but considering only P^+ alleles present in founder P^+ cells (i.e., excluding P^+ alleles present in recipient cells because of transfer).

Statistical analysis. Differences between conditions with and without transfer were tested with two-sample, two-sided t tests. The normality of distributions was confirmed with Shapiro–Wilkinson tests, rejecting the null hypothesis when $P < 0.05$. When normality was rejected, the nonparametric Wilcoxon signed-rank test was used instead of the t test.

Mathematical Modeling. ***Within-population dynamics.*** We model the dynamics of producer (P^+) and nonproducer (P^-) alleles, carried on horizontally transmitted, incompatible plasmids. Plasmids can be transferred to plasmid-free recipient cells (R) only, assuming entry exclusion between incompatible plasmids (10). Producer cells (that bear P^+ plasmid) pay a cost of cooperation c, nonproducers (P^- cells bearing P^- plasmid and plasmid-free R cells) do not. Transfer follows a mass-action law (11): the number of transfer events depends on the frequency of encounters between donor and recipient cells, assumed to be proportional to both donor cell (P^+ or P^-) and recipient cell (R) densities in the local population. The transfer rate constant γ (mL cell^{-1}·h^{-1}) describes the plasmid ability to transfer, and is expressed as the number of events per concentration (cell/mL), per unit time (h). Here, P^+ and P^- have transfer rates γ_{P+} and γ_{P-} respectively. We neglect plasmid loss, the effects of which are generally low compared with growth rate effects (12).

Growth follows a logistic function with cell densities saturating at a carrying capacity K, mimicking growth to stationary phase with the progressive consumption of resources (and neglecting cell death and turnover at this timescale of hours). We have chosen the specific mathematical form of our model to follow our experimental setup where cells grow in finite, exhaustible media (unlike a "chemostat" setting, often used for model simplification). If the population was then left in that state for a longer period, the individuals would start dying and a potentially more complex dynamic could develop over a much slower timescale. However, as our experiments are carried out in the timescale of hours, such long-term processes are not relevant.

Transfer saturates in the same way as growth, at carrying capacity K, as F transfer has been shown to strongly decrease when cells approach stationary phase (13).

The costs and benefits of public good production act solely on growth rate, as the public good does not liberate any additional resources and thus does not provide any enhancement to the carrying capacity. The carrying capacity is the same for all genotypes and is not affected by the presence of Cm (1) or the public goods (confirmed by experimental measurements for our modified strains, if the time of growth is extended beyond the one used in our experiments in the presence of Cm).

We explicitly follow the experimental setup by modeling its two steps. From t_0 to t_1, preinduction of Cm resistance and transfer happen until stationary phase similarly to experiments, without effects of public goods except their cost. The basal growth rate during this step is the constant rate ψ_1. From t_1 to t_2, the growth rate depends on the benefit of public goods b and on the public good concentration, assumed to be proportional to the proportion of producing cells in the local population P^+/n_{tot}. The basal growth rate during this step is ψ_2, which depends on the proportion of producers as follows: $\psi_2 = \psi_0 \times (1 + b \times P^+/n_{tot})$.

General equations for growth and transfer, which we present directly below, are common to the two steps (substituting, respectively, ψ_1 for ψ, from t_0 to t_1, and ψ_2 for ψ, from t_1 to t_2). We modeled two cases, with or without amplification of transfer by recipients that become secondary donors.

In the first case (all simulations except Fig. 5*B*), we model self-transfer of conjugative plasmids where conjugation controlling genes are also transferred (14), with amplification of transfer in recipients. This corresponds to the dynamics of plasmids in our experiments: with our experimental setup (Fig. 1*A*), conjugation genes from F_{HR} plasmid are not transferred but present in all cells, so conjugation is effectively controlled by *oriT* presence on transferred plasmids, making them similar to conjugative plasmids. Initial and secondary plasmid donors are not distinguished in the model.

$$\frac{dP^+}{dt} = [\psi(1-c) + \gamma_{P^+}R]P^+\left(1 - \frac{n_{tot}}{K}\right),$$

$$\frac{dP^-}{dt} = [\psi + \gamma_{P^-}R]P^-\left(1 - \frac{n_{tot}}{K}\right),$$

$$\frac{dR}{dt} = [\psi - (\gamma_{P^+}P^+ + \gamma_{P^-}P^-)]R\left(1 - \frac{n_{tot}}{K}\right).$$

In the second case (Fig. 5*B*), we assume that no secondary transfer happens from recipient cells. We thus model mobilization by factors present in the initial hosts, but not the secondary hosts (15). Initial plasmid bearers (I: IP^+ bearing P^+ plasmid and IP^-

bearing P^- plasmid) and recipients (noted R, RP^+, and RP^-, respectively, for plasmid-free, P^+-bearing, and P^--bearing recipient cells) are considered as separate genotypes, with $P^+ = IP^+ + RP^+$ and $P^- = IP^- + RP^-$:

$$\frac{dIP^+}{dt} = \psi(1-c)IP^+\left(1-\frac{n_{tot}}{K}\right),$$

$$\frac{dIP^-}{dt} = \psi IP^-\left(1-\frac{n_{tot}}{K}\right),$$

$$\frac{dR}{dt} = [\psi - (\gamma_{P^+}IP^+ + \gamma_{P^-}IP^-)]R\left(1-\frac{n_{tot}}{K}\right)$$

$$\frac{dRP^+}{dt} = [\psi(1-c)RP^+ + \gamma_{P^+}IP^+R]\left(1-\frac{n_{tot}}{K}\right),$$

$$\frac{dRP^-}{dt} = (\psi RP^- + \gamma_{P^-}IP^-R)\left(1-\frac{n_{tot}}{K}\right).$$

Metapopulation structure and selection. For the simulations presented in Fig. 2, the population is a well-mixed population.

We then model two types of metapopulations containing multiple separate populations.

For all other simulations except the one presented in Fig. 6, we model a simple metapopulation consisting of two separate populations that differ in their initial ratio of P^+ to P^- plasmids (t_0), and share the same proportion of R cells.

For simulations presented in Fig. 6, we model a metapopulation with 96 subpopulations where founder cells arise from a strongly diluted common mix of cells, giving rise to a Poisson distribution for each type of cell (1). This leads to stochastic variation in producer frequencies among subpopulations, and is generally similar to earlier models of cooperation via stochastic variation in compartmentalized populations (16).

Populations grow separately until t_2, where all populations are pooled. For Fig. S4, plasmid-bearing cells that arose from transfer (RP^+ and RP^-) were distributed in equal proportions in the two populations at t_1, keeping all other population parameters constant, and relatedness was computed after mixing. For Fig. S5, additional migration was modeled between the two populations at t_1 (after transfer): the migration rate is equal to the proportion of cells of each population that migrates to the other population at the t_1 time point.

To analyze the effect of pure infectious transfer (Fig. 2), changes in P^+ proportion were computed from t_0 to t_1 (as the public good benefits do not play a role in the infectious transfer hypothesis, and transfer happens efficiently from t_0 to t_1). When cooperation was involved (all other simulations), changes in P^+ proportion were computed from t_1 to t_2 (when public goods affect growth). As the public good acts on growth rate, the benefit of cooperation is only transient (1) and t_2 has to be chosen before all populations reach stationary phase. For each simulation, t_2 is defined as the time point where the selection of P^+ is maximal over all conditions tested.

Parameter values. Parameters values used in all models are shown below and were estimated from our experimental data:

Carrying capacity	$K = 4\times10^9$ cells mL^{-1}
Basal growth rate in the absence of Cm	$\psi_1 = 0.96\ h^{-1}$
Basal growth rate in the presence of Cm	$\psi_0 = 0.12\ h^{-1}$
Cost of public good production	$c = 0.04$
Benefit of cooperation on growth rate	$b = 4.$

The rates of transfer γ_{P^+} and γ_{P^-} were varied from 0 to 2×10^{-9} mL $cell^{-1}\cdot h^{-1}$, which encompasses the range of transfer rates that can be measured, and knowing that derepressed plasmids transfer at a rate around 10^{-9} mL $cell^{-1}\cdot h^{-1}$ (17). The rate was divided by 10 in the presence of Cm, to mimic experiments where growth in Cm happens at 30 °C and transfer is reduced. We did not attempt to measure γ experimentally, as the transfer rate is not constant during the duration of the experiments (because of successive dilutions and shifts in temperature). However, we can estimate an effective transfer rate that would lead to the plasmid invasion that was observed at t_1 in experiments. The measured effective transfer rates vary from 5×10^{-10} mL $cell^{-1}\cdot h^{-1}$ to 10^{-9} mL $cell^{-1}\cdot h^{-1}$ in our experiments.

The preincubation time was set to 12 h after 100-fold initial dilution from stationary phase cultures at carrying capacity, and growth in the presence of the antibiotic was allowed for 60 h after a second 100-fold dilution.

To study the effect of strong cell dilution (Fig. 6), cells were distributed in 96 populations each of 10 μL, following a Poisson distribution of parameter λ (P^+ and P^-) and 98 λ (R), ensuring an initial proportion of 2% plasmids. λ was varied from 1 to 15. Because of the strong initial dilution, the preincubation time was set at 24 h and a second 10-fold dilution step was added before t_1. Results were averaged over 20 replicate simulations, as strong variance arises from Poisson distribution.

All computer simulations were conducted using MATLAB.

1. Chuang JS, Rivoire O, Leibler S (2009) Simpson's paradox in a synthetic microbial system. *Science* 323(5911):272–275.
2. Anthony KG, Sherburne C, Sherburne R, Frost LS (1994) The role of the pilus in recipient cell recognition during bacterial conjugation mediated by F-like plasmids. *Mol Microbiol* 13(6):939–953.
3. Stern JC, Schildbach JF (2001) DNA recognition by F factor TraI36: highly sequence-specific binding of single-stranded DNA. *Biochemistry* 40(38):11586–11595.
4. Achtman M, Kennedy N, Skurray R (1977) Cell—cell interactions in conjugating *Escherichia coli*: role of traT protein in surface exclusion. *Proc Natl Acad Sci USA* 74(11):5104–5108.
5. Elowitz MB, Levine AJ, Siggia ED, Swain PS (2002) Stochastic gene expression in a single cell. *Science* 297(5584):1183–1186.
6. Registry of Standard Biological Parts http://parts.igem.org/.
7. Philippe N, Alcaraz J-P, Coursange E, Geiselmann J, Schneider D (2004) Improvement of pCVD442, a suicide plasmid for gene allele exchange in bacteria. *Plasmid* 51(3): 246–255.
8. Datsenko KA, Wanner BL (2000) One-step inactivation of chromosomal genes in *Escherichia coli* K-12 using PCR products. *Proc Natl Acad Sci USA* 97(12):6640–6645.
9. Gardner A, West SA, Wild G (2011) The genetical theory of kin selection. *J Evol Biol* 24(5):1020–1043.
10. Garcillán-Barcia MP, de la Cruz F (2008) Why is entry exclusion an essential feature of conjugative plasmids? *Plasmid* 60(1):1–18.
11. Levin BR, Stewart FM, Rice VA (1979) The kinetics of conjugative plasmid transmission: fit of a simple mass action model. *Plasmid* 2(2):247–260.
12. Lau BTC, Malkus P, Paulsson J (2013) New quantitative methods for measuring plasmid loss rates reveal unexpected stability. *Plasmid* 70(3):353–361.
13. Frost LS, Manchak J (1998) F- phenocopies: Characterization of expression of the F transfer region in stationary phase. *Microbiology* 144(Pt 9):2579–2587.
14. Stewart FM, Levin BR (1977) The population biology of bacterial plasmids: A priori conditions for the existence of conjugationally transmitted factors. *Genetics* 87(2): 209–228.
15. Levin BR, Stewart FM (1980) The population biology of bacterial plasmids: A priori conditions for the existence of mobilizable nonconjugative factors. *Genetics* 94(2): 425–443.
16. Szathmáry E, Demeter L (1987) Group selection of early replicators and the origin of life. *J Theor Biol* 128(4):463–486.
17. Simonsen L (1991) The existence conditions for bacterial plasmids: Theory and reality. *Microb Ecol* 22(1):187–205.

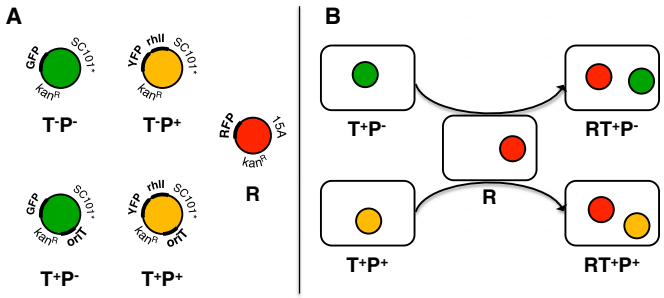

Fig. S1. Plasmids used in experiments and strain identification. Plasmids are colored according to the fluorescence genes they bear. (*A*) Plasmids used in experiments. pSC101-origin (pSC101*) bearing plasmids are responsible for transfer and production phenotypes. P^- and P^+ indicate public good production status: P^+ plasmids express RhlI synthase and YFP; P^- plasmids express only GFP. T^- and T^+ indicate transfer status, T^+ are transferable as they bear F *oriT*. Recipients bear a compatible plasmid (with p15A replication origin) expressing RFP. p15A-origin and pSC101-origin bearing plasmids all bear a kanamycin resistance gene (kan^R). (*B*) Identification of strains and plasmids with plasmid fluorescence genes. Initial strains are marked with only one fluorescence plasmid (the case of T^+ plasmids is represented here). With transfer, recipients bearing two plasmids arise, and are identified by the combination of RFP and GFP or RFP and YFP fluorescence.

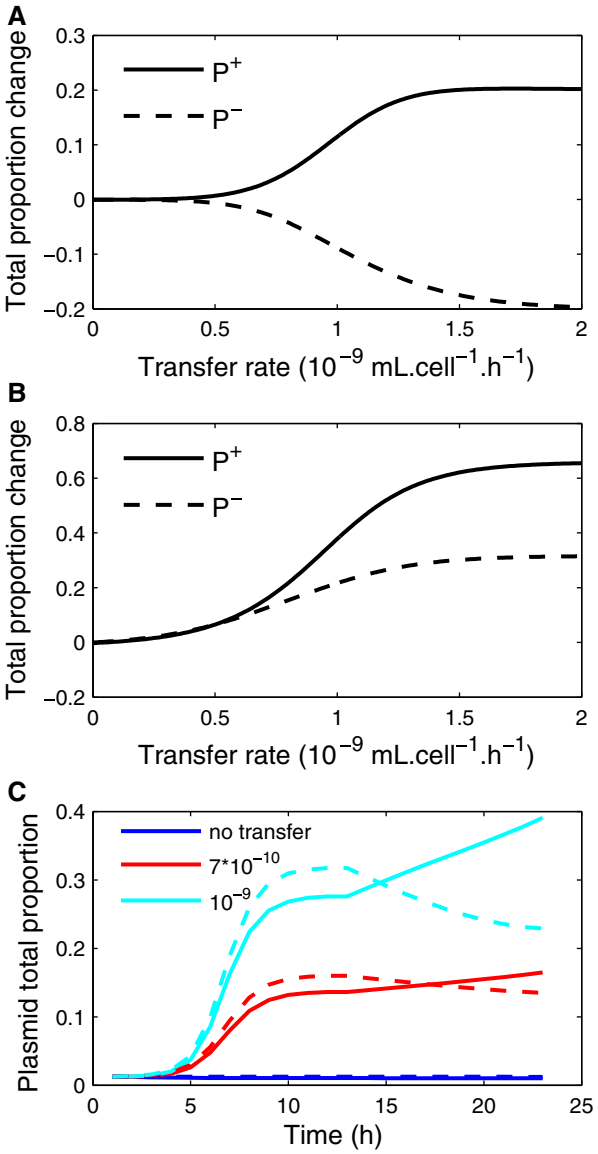

Fig. S2. Dynamics of plasmids in the total metapopulation. The metapopulation is the same as in Fig. 3. The changes in proportion of P^+ and P^- in the total population [respectively, $P^+/(P^+ + P^- + R)$, plain lines, and $P^-/(P^+ + P^- + R)$, dashed lines] are computed in simulations from t_1 to t_2 (*A*) and from t_0 to t_2 (*B*) as a function of the common transfer rate of P^+ and P^-. Infectious transfer takes place mainly from t_0 to t_1; public goods affect population growth from t_1 to t_2. As an example, plasmid proportions are also shown as a function of time (*C*) in the absence of transfer (blue), for a transfer rate of 7×10^{-10} mL $cell^{-1} \cdot h^{-1}$ (that corresponds to the estimated experimental transfer rate, red) and a transfer rate of 10^{-9} mL $cell^{-1} \cdot h^{-1}$ (cyan).

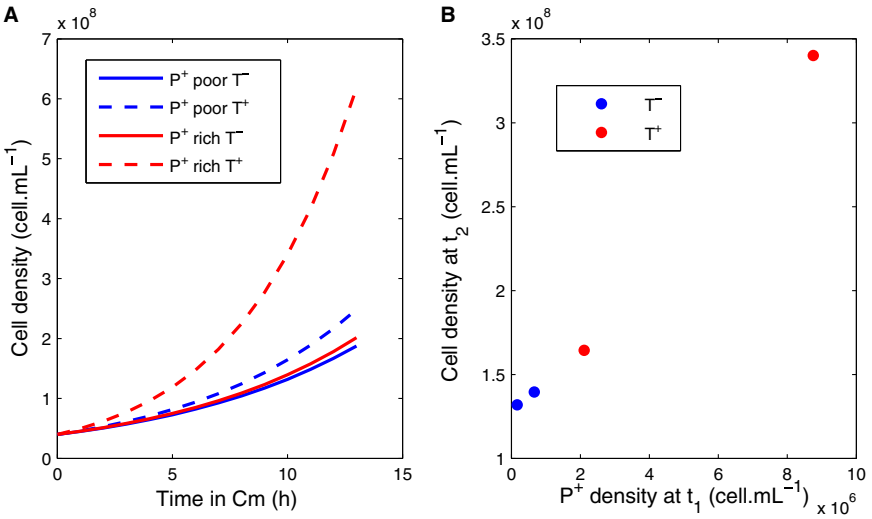

Fig. S3. Growth of subpopulations in the presence of Cm. The total cell density is computed in simulations for P^+-poor (blue) and P^+-rich (red) populations, in the absence (T^-) or presence (T^+) of transfer at a rate of 7×10^{-10} mL cell^{-1}·h^{-1} (that corresponds to the estimated experimental transfer rate). Parameters are the same as in Fig. 3. In *A*, the total density is shown as a function of time in the presence of Cm (from t_1 to t_2). In *B*, the total density is shown at t_2 as a function of P^+ density at t_1 (after most of the transfer happened).

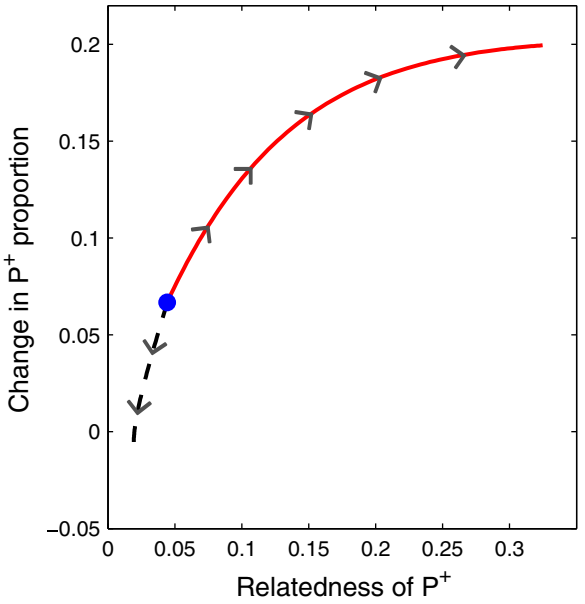

Fig. S4. Transfer selects for cooperation by increasing assortment among P^+ alleles. Parameters are the same as in Fig. 3, except recipient's proportion, which is 75%. The simulated change in P^+ proportion is shown as a function of P^+ relatedness, with transfer within populations (solid red line) or randomized across populations (dashed black line). Arrows indicate the direction of increasing transfer rates, the blue dot indicating absence of transfer.

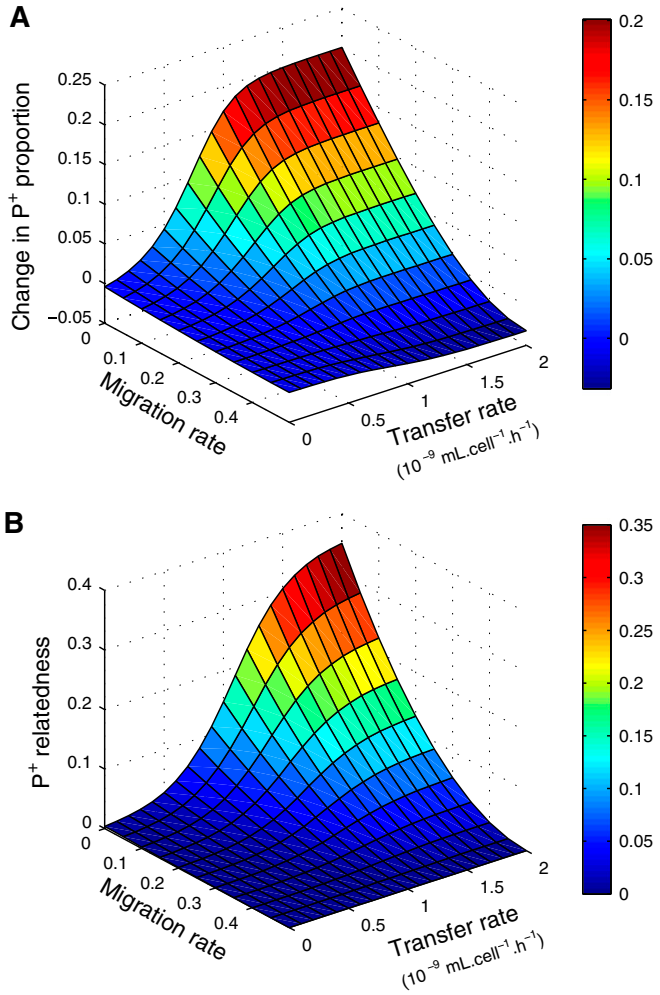

Fig. S5. Transfer and migration have antagonistic effects on the selection of cooperation. The metapopulation consists of two subpopulations, with initial P^+/P^- ratio of 1:4 and 4:1. The surface represents the change in proportion of P^+ among all plasmids $P^+/(P^+ + P^-)$ in the presence of Cm (from t_1 to t_2) (*A*) and P^+ relatedness at t_1 (*B*), as a function of the common transfer rate of P^+ and P^- plasmids and of the migration rate between the two populations (proportion of cells that are exchanged between the two populations at t_1).